doi:10.15625/2525-2518/21965

Convergence of complex multi-variables based on fading channels in multi-antenna communication systems

Pham Anh Thu¹, Nguyen Duc Minh², Le Hai Chau^{1,2}, Hoang Trong Minh^{1,*}

¹Faculty of Telecommunications, Posts and Telecommunications Institute of Technology, Km10 Nguyen Trai Road, Ha Dong, Hanoi 10000, Viet Nam

²Data and Intelligent Systems Laboratory, Posts and Telecommunications Institute of Technology, Km10 Nguyen Trai Road, Ha Dong, Hanoi 10000, Viet Nam

*Email: hoangtrongminh@ptit.edu.vn

Received: 17 November 2024; Accepted for publication: 23 May 2025

Abstract. This work introduces approximate expressions and provides comprehensive simulation results to demonstrate the robust convergence of complex variables based on fading channels in multi-antenna communication systems, in which two separate scenarios, namely spatial signal processing and non-spatial signal processing scenarios, were evaluated. Numerical results prove our assertions that for Nakagami-*m* and Rician fading channels (or can be extended to any other complex fading channels) in multi-antenna systems with antenna numbers larger than two, the distribution of interference from the beamforming design, a typical example for spatial signal processing, and will strongly converge to an exponential distribution with the scale-parameter remaining the same. Meanwhile, the channel synthesis in the non-spatial signal processing scenario tends to an exponential distribution with a new scale parameter exactly equal to the product of the number of antennas and the scale parameter.

Keywords: wireless communication, MIMO, multi-antenna, fading channels.

Classification numbers: 2.4.2, 2.4.4, 5.2.1.

1. INTRODUCTION

The proliferation of fifth-generation (5G) and beyond wireless networks, along with enhanced latency reduction techniques and optimised bandwidth allocation methods, has led to dramatic increases in per-user device connectivity [1-3]. The significant rise is largely due to the extensive deployment of the Internet of Things (IoT), which includes environmental sensors, wearable computing devices, and industrial automation systems. These developments demands robust and flexible wireless network architectures to meet growing connectivity requirements [4]. The intensifying demand introduces multifaceted challenges for network infrastructure, particularly with multiple or large antenna transmitters in high-density deployment scenarios

where numerous users and devices compete for limited spectral resources. The ongoing increase in devices presents network operators with the challenge of ensuring sufficient bandwidth allocation and maintaining latency for each endpoint while preserving overall system performance metrics [3, 5].

To maintain pace with the technological advancement in signal transmission, the need to control and amplify signals to maximize transmission is in high demand [6, 7]. Signal processing techniques in multi-antenna wireless systems optimise data transmission, reduce interference, and enhance system dependability, particularly in complex fading environments. Interference management is a major challenge. In the spatial optimisation scenario, beamforming and precoding are used to direct signals to specific users and minimise spillover [8]. These methods decrease co-channel interference and increase user signal quality by targeting signal energy. In crowded areas with many users, interference management is difficult and typically requires sophisticated spatial strategies like coordinated beamforming or interference-aware precoding to maintain performance. Equalisation, frequency-domain processing as OFDM, and interference management use time and frequency domain methods to tackle interference without spatial directionality [9]. A comprehensive investigation of these challenges demands detailed implementation. However, current research has mostly evaluated, estimated, or approximated interference using zero-mean Gaussian random variables and the central limit theorem (CLT) [10, 11]. Pre-coding and other methods aim for high speed, low latency, low cost, and reliable signal broadcast. A minimization-maximization algorithm to optimise the down-link sum rate has been proposed in [12], where an enhanced pre-coding vector handled each user's transmit signals. Beamforming design is also widely used. In MIMO systems with moderate numbers of antennas, beam-forming reduced correlated noise and interference [13]. However, traditional approaches operate well under ideal circumstances, but real-world applications typically include numerous users sending or receiving signals concurrently, reducing performance. In complicated multi-user systems, when interference and spatial correlations increase, pre-coding and beamforming might become more pronounced [14]. This is exceptionally difficult in large-scale MIMO systems, where the number of users increases and signal optimization becomes a more nuanced difficulty. As a result, the ability to precisely control and direct signals toward multiple users while minimizing cross-user interference diminishes, leading to a degradation in signal quality for non-targeted users. Moreover, [15] presented a minimization-maximization algorithm to optimise the downlink sum rate utilising an advanced pre-coding vector for user signals. Nevertheless, these methods face limitations in multi-user environments. Traditional precoding and beam-forming techniques struggle to handle cross-user interference, lowering signal quality. Additionally, switching or all-antenna-on approaches without channel state information (CSI) yield suboptimal energy and performance, particularly in highly correlated or crowded signal environments. Consequently, a thorough analysis is necessary to address the multiple aforementioned issues. However, recent scientific researches only commute an estimation to zero-mean Gaussian random variables via CLT, as discussed in [16-19]. Particularly, the authors in [17] employed the CLT to examine the variability of mutual information in large MIMO systems with elliptically correlated channels. Similarly, [20] applied the classical CLT to model Locational Marginal Pricing (LMP) in power systems.

Typically, hundreds to thousands or even tens of thousands of sophisticated random components are needed to meet the CLT criteria. This requirement raises concerns about the validity of the results in the prior research, particularly in practical scenarios where the number of antennas ranges from 2 to 10. When considered within the CLT framework, systems that support low to high antenna numbers provide exhibit inconsistent results. CLT efficacy depends on the quantity of random variables, according to recent studies [10] and [11]. As a result, this

method depends on a number of variables to ensure various reliable outcomes. From these observations, the inherent limitations of relying on CLT in practical schemes become evident. CLT-based models do not adequately represent the performance of systems with fewer random variables, such as those with low antenna arrays, resulting in not certain accuracy. Therefore, the robustness of the conclusions from mentioned studies is limited when applied to systems with lower antenna counts or when attempting to design flexible systems that span a broad range of antenna configurations.

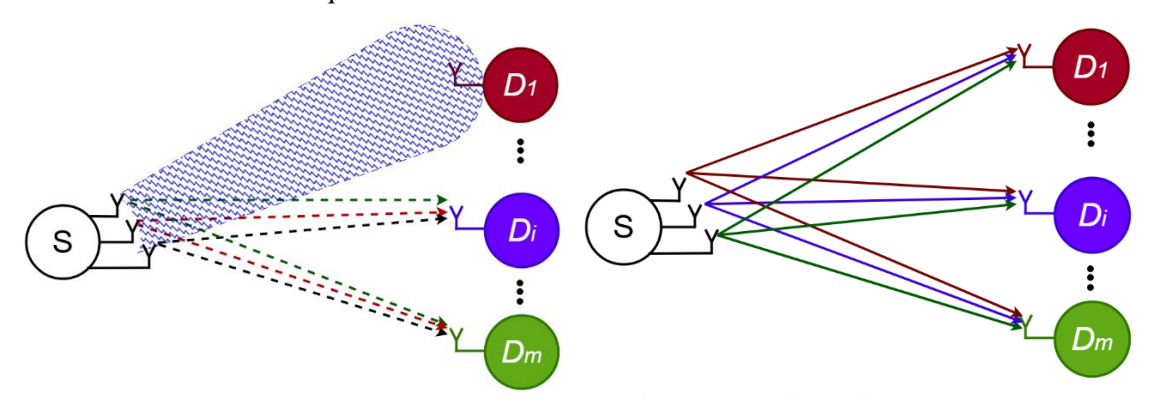
Motivated by these drawbacks, in this paper, we propose a closed-form expression-based estimation of the consistent convergence patterns of complex variables in multi-antenna communication systems experiencing fading channels, delivering high accuracy even with few element antenna arrays. We investigate two distinct scenarios: one involving spatial signal processing and another without it (so-called non-spatial signal processing), under both Nakagami-m and Rician fading channels. Under both Nakagami-m and Rician fading channels, the interference distribution from the spatial signal processing scheme exhibits strong convergence to an exponential distribution while maintaining its scale parameter while the channel synthesis of the non-spatial signal processing scenarios also approaches an exponential distribution, but with a modified scale parameter that equals the original scale parameter multiplied by the number of antennas. Due to current mathematical limitations, the proposed estimation models are verified by utilizing comprehensive numerical simulations. The simulation results prove that the convergence of individual channels, whether they follow the Nakagami-m or Rician fading models, transitions to an exponential distribution, achieving high accuracy even in the scenario with only two antennas. This level of precision is notable, as achieving such a result with CLT is nearly impossible due to the insufficient number of antenna elements. In our investigated scenarios, all results demonstrate that convergence occurs quickly and efficiently even under varying input configuration parameters. This demonstrates the robustness of the assumed model in handling low-element configurations. These results offer insights into the behavior of complex fading channels in multi-antenna systems and hold significant implications for system design and performance evaluation.

2. CONSIDERED SCENARIOS

2.1. Problem statement

In multi-antenna wireless systems, signal processing techniques can be categorized into spatial and non-spatial processing, each offering distinct approaches to optimizing communication performance. Spatial processing primarily employs beamforming and precoding techniques, which enhance transmission quality by strategically directing signal energy toward intended users while minimizing interference. These methods leverage channel state information to maximize signal strength at the receiver, thereby improving system reliability, data rates, and spectral efficiency. Through precise adjustment of signal directionality and structure, the transmitting device can effectively counteract fading and noise in complex environments. However, this approach creates a performance disparity: while the primary user experiences significant gains, secondary users often face limited performance improvements, regardless of increases in the number of transmit antennas. In contrast, non-spatial processing encompasses techniques such as equalization, diversity combining, and interference management, where signals are broadcast without spatial optimization. This approach typically results in more uniform performance gains across all users as the number of antennas increases, differing from

spatial processing's pattern of concentrated enhancement for the primary user. The non-spatial approach offers greater flexibility and versatility in optimizing system performance, particularly in scenarios where spatial processing may be impractical or inefficient. Together, these complementary processing strategies provide system designers with diverse options for enhancing multi-antenna wireless communications, allowing adaptation to various channel conditions and network requirements.



a) Spatial signal processing scenario b) Non-spatial signal processing scenario Figure 1. Illustration of the considered system models.

Accordingly, a typical multiple antenna system model is considered, where a source (S) with T antennas is communicating to M single antenna devices ($D_1, D_2, ..., D_M$) (or another typical name is a multi-user MISO system) as illustrated in Figure 1 with T>1 and M>1. Herein, the fading channel from $i \in \{1, ..., T\}$ -th antenna of S to $j \in \{1, ..., M\}$ device is modeled by Nakagami-m and Rician, respectively, as

$$f_{\left|h_{S_{i}D_{j}}\right|^{2}}^{Naka}(x) = \frac{x^{m_{SD_{j}}-1}}{\Omega_{SD_{j}}\Gamma(m_{SD_{j}})} \exp\left(\frac{-x}{\Omega_{SD_{j}}}\right)$$
(1)

$$f_{\left|h_{S_{i}D_{j}}\right|^{2}}^{Rici}(x) = \frac{2\left(K_{SD_{j}}+1\right)x}{\Omega_{SD_{j}}} \exp\left(-K_{SD_{j}}-\frac{\left(K_{SD_{j}}-1\right)x^{2}}{\Omega_{SD_{j}}}\right) I_{0}\left(\sqrt{\frac{K_{SD_{j}}\left(K_{SD_{j}}+1\right)}{\Omega_{SD_{j}}}x}\right), \quad (2)$$

where Ω_{SD_j} is the scale parameter, K_{SD_j} is the Rician K factor, m_{SD_j} is the fading parameter, $I_0(.)$ is the 0-th order modified Bessel function of the first kind, and $\Gamma(.)$ is the gamma function. Accordingly, interference from beam-forming design and uncontrolled signal scenarios are considered, since the beam-forming vector at S cannot be aligned for all devices simultaneously for downlink models and S also cannot determine individual signals in a complex mixture without control when considering practical or mathematical designs.

2.2. Spatial signal processing scenario

To take full advantage of downlink system performance, a beam-forming vector design is introduced at S, as depicted in Figure 1(a). However, considering a practical scenario, only one user is served by a beamforming vector, while other users receive a signal with interference from beam-forming designs as mentioned above. For an example, the beam-forming vector for D_I can be designed as $\mathbf{w}_{SD_1}^{\dagger} = \mathbf{h}_{SD_1}^{\dagger} / \|\mathbf{h}_{SD_1}\|$ with $\mathbf{h}_{SD_1} = [\mathbf{h}_{S_1D_1}, ..., \mathbf{h}_{S_MD_1}]$ and a conjugate transpose $\mathbf{h}_{SD_1}^{\dagger}$, accordingly, the received channel gains at D_I and D_j with $j \neq 1$ can be expressed,

respectively, as

$$\left|\mathbf{h}_{SD_1} w_{SD_1}^{\dagger}\right|^2 = \frac{\left|\mathbf{h}_{SD_1} w_{SD_1}^{\dagger}\right|^2}{\left\|\mathbf{h}_{SD_1}\right\|^2} = \left\|\mathbf{h}_{SD_1}\right\|^2$$
 (3)

$$\left|\mathbf{h}_{SD_{j}}\mathbf{w}_{SD_{1}}^{\dagger}\right|^{2} = \frac{\left|\mathbf{h}_{SD_{j}}\mathbf{w}_{SD_{1}}^{\dagger}\right|^{2}}{\left\|\mathbf{h}_{SD_{j}}\right\|^{2}}.$$
 (4)

Herein, the CDF/PDF of (3) can be easily conducted as in previous studies, while the general solution for CDF/PDF of (4) still remains an open question. Note that some works as in [13, 14] introduced that (4) will tend to zero-mean Gaussian random variable based on the center limit theorem (CLT). However, CLT implies a sufficiently large T, which is not convincing for a small value of T. Accordingly, we propose a general solution for the CDF/PDF of (4) as

$$F_{\left|\mathbf{h}_{SD_{i}}\mathbf{w}_{SD_{1}}^{\dagger}\right|^{2}}(x) = \mathbf{1} - \exp\left(\frac{-x}{\Omega_{SD_{i}}}\right),\tag{5}$$

$$f_{\left|\mathbf{h}_{SD_{j}}\mathbf{w}_{SD_{1}}^{\dagger}\right|^{2}}(x) = \frac{1}{\Omega_{SD_{j}}} \exp\left(\frac{-x}{\Omega_{SD_{j}}}\right). \tag{6}$$

2.3. Non-spatial signal processing scenario

The second scenario considers a non-spatial signal processing scenario, as shown in Figure 1(b), where the source device communicates with devices without applying/using any signal control technique. Note that our main focus is on estimating complex random variables of complex fading channels, in this scenario, the signal quality of all users is improved proportionally by increasing the number of antennas at the source. This is because only one user is strongly enhanced by using the beamforming design, while the performance of other users is not improved, regardless of the increase in the number of antennas as shown in (5). However, the improvement is only marginal and not as strong as in the single-user beamforming design scenarios. Mathematically, the received channel gain at j-th D from S can be expressed as

$$\left|\mathbf{h}_{SD_j}\right|^2 = \left|\mathbf{h}_{S_1D_j} + \dots + \mathbf{h}_{S_TD_j}\right|^2. \tag{7}$$

However, to derive an exact CDF/PDF for $\left|\mathbf{h}_{SD_{j}}\right|^{2}$ is an impossible mission. Then, some recent works presented an approximation approach based on CLT, as a zero-mean Gaussian random variable. Similar to the first scenario (spatial signal processing), CLT is not sufficient for small values. Therefore, by rewriting $\left|\mathbf{h}_{SD_{j}}\right|^{2} = \left|\mathbf{M}\mathbf{h}_{SD_{j}}\right|^{2}$, we propose a general approach for the CDF/PDF of $\left|\mathbf{h}_{SD_{j}}\right|^{2}$ as

$$F_{\left|\mathbf{h}_{SD_{j}}\right|^{2}}(x) = 1 - \exp\left(-\frac{x}{M\Omega_{SD_{j}}}\right),\tag{8}$$

$$f_{\left|\mathbf{h}_{SD_{j}}\right|^{2}}(x) = \frac{1}{M\Omega_{SD_{j}}} \exp\left(\frac{-x}{M\Omega_{SD_{j}}}\right).$$
 (9)

In our proposals, the CDFs/PDFs in (5)/(6) and (8)/(9) converge to the exponential distributions, where the scale parameter of (5)/(6) remains the same and the scale parameter of (8)/(9) is updated to equal the product of the number of complex variables and the scale parameter. Notably, the exponential distribution is easier than the next mathematical step for the complex system models when compared to the zero-mean Gaussian distribution, as assertions in the previous works as

$$f(x) = \frac{1}{\sqrt{\pi \sigma}} \exp\left(-\frac{x^2}{2\sigma^2}\right),\tag{10}$$

where σ^2 is the variance of the random variable x. As observed, (10) including x^2 , leading to a certain mathematical complexity. Furthermore, (10) is estimated relatively through CLT, where the question "how many components are enough?" is considered as an open question. However, it cannot be proven mathematically, and the accuracy is verified by comprehensive simulations.

3. SIMULATION RESULTS

In this section, we provide comprehensive results based on 10⁷ samples of the Monte-Carlo simulations to corroborate our assertions. All simulation parameters are set as in Table 1. As can be observed, all simulation results (Sim.) in Figures 2 to 5 well match our proposed method, demonstrating the high accuracy of our approach (Assumption), regardless of the variety of parameters.

| Parameters | Symbols | Symbols Values |
|-------------------------------------|----------------------|------------------------|
| Number of antennas | T | 1, 3, 6, 9, 20, and 50 |
| Scale parameter | $\Omega_{SD_{m{j}}}$ | 0.5, 1, 2, and 4 |
| Nakagami- <i>m</i> fading parameter | m_{SDj} | 0.5, 1, 2, and 4 |
| Rician K factor | K_{SDi} | 0, 3, and 9 |

Table 1. Variety of simulation parameters.

3.1. Spatial signal processing scenario

Figure 2 examines the PDFs of the received channel at D_j under varying antenna settings $T = \{1, 3, 6, 9, 20, 50\}$, scale parameter $\Omega_{SD_j} = \{0.5, 1, 2, 4\}$, and $m_{SD_j} = \{0.5, 1, 2, 4\}$ for Nakagami-m fading channels, and $K_{SD_j} = \{0, 3, 9\}$ for Rician fading channels. As can be observed, all results indicate some interesting points as:

• For T=1 in Figure 2(a), the PDF of channels from S to D_j follows the original distributions based on the fading channels, where Nakagami-m fading channels are captured by the fading condition through its shape parameter m_{SD_j} and Rician fading channels are characterized by K_{SD_j} , since beamforming design is not applicable in single-antenna systems. As for T=3, the simulation results show a slightly smaller at small x and a slightly larger at large x when compared to the PDF results for $\left|\mathbf{h}_{SD_j}\mathbf{w}_{SD_j}^{\dagger}\right|^2$ based on our statement. However, when

considering in overall view, the difference between the simulation results and our approaches is almost insignificant. Notably, as observed, the gap between the simulation results for T=3 and T=9 is almost negligible, demonstrating the strong convergent of $\left|\mathbf{h}_{SD_{j}}\mathbf{w}_{SD_{j}}^{\dagger}\right|^{2}$ to the exponential distribution.

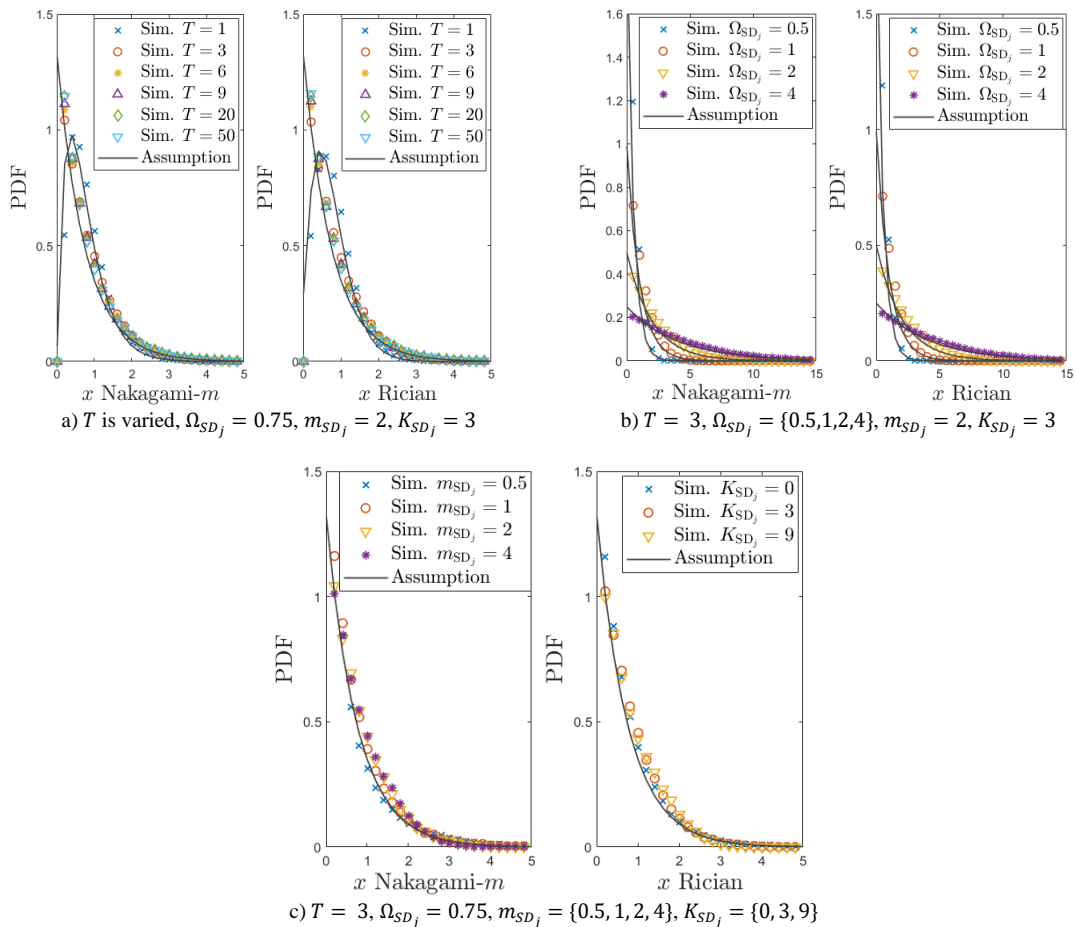


Figure 2. PDF for interference in spatial signal processing scenario.

- Figure 2(b) illustrates the simulated and theoretical channel PDFs in which T is set at 3, m_{SD_j} is equal to 2, K_{SD_j} is 3, and Ω_{SD_j} is varied in the set of {0.5, 1, 2, 4}. The graphs imply that the PDFs tend to follow an exponential distribution with the same scale parameter, and the simulation results properly match that of the proposed theoretical analysis.
- Particularly, Figure 2(c) demonstrates the PDF of the channel from S to D_j with T of 3, Ω_{SD_j} of 0.75 while $m_{SD_j} = \{0.5, 1, 2, 4\}$ and $K_{SD_j} = \{0, 3, 9\}$ respectively for Nakagami-m fading channels and Rician fading channels. The obtained results again confirm that the channel gain from S to D_j also complies with the trend in Figure 2(a) with $T \neq 1$. There are minor variations between the simulated and theoretical PDFs of $\left| \mathbf{h}_{SD_j} \mathbf{w}_{SD_j}^{\dagger} \right|^2$. A proper match between these PDFs is verified even with small x and the deviation is negligible when

considering the overall distribution pattern. In other words, the $\left|\mathbf{h}_{SD_j}\mathbf{w}_{SD_j}^{\dagger}\right|^2$ strongly complies with and rapidly converges to the exponential distribution.

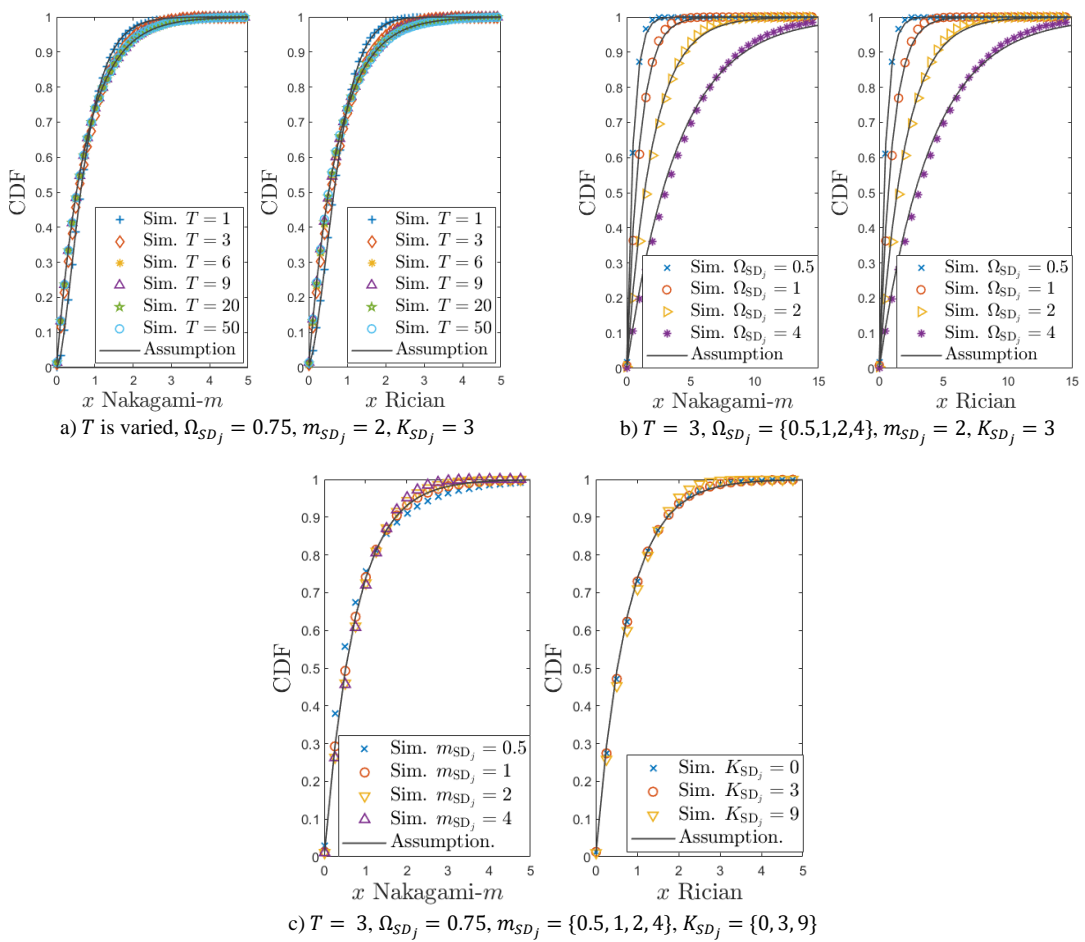


Figure 3. CDF for interference in spatial signal processing scenario.

Although the above results have shown a useful result for the PDF of (4), however, to have a more comprehensive observation when estimating a distribution, the results for the CDF of (4) have been presented in Figure 3. Accordingly, the effects of T, Ω_{SD_j} , and m_{SD_j} as well as K_{SD_j} on the CDF of (5) are piloted in Figures 3(a), (b), and (c), respectively, where the simulation results match (5) perfectly. Specifically, as discussed in the PDF results, the simulation results for T=1 follow the principle of Nakagami-m and Rician fading channels, while T=3 and T=9 present a strong convergent to an exponential distribution with the scale parameter is not changed. Not only that, the curve gap between the simulation results for T=3 and T=9 is almost negligible, confirming our observation that a small T is sufficient for (4) to converge. Mathematically, only the varying setting of T is not enough for our statement, the difference value of scale parameter Ω_{SD_j} is examined in Figure 3(b). Herein, (5) once again is confirmed by the simulation results. Notably, when exploring the difference value of Ω_{SD_j} , the characteristic of (5) will be changed, since the distribution depends on the scale parameter. Later, the effect of m_{SD_j} and K_{SD_j} , two importance parameters of Nakagami-m and Rician fading channels, are

illustrated in Figure 3(c). All results introduce an interesting point that the CDF of the interference from beamforming design can be approximated as an exponential distribution, regardless of the varying setting of m_{SD_i} and K_{SD_i} .

3.2. Non-spatial signal processing scenario

To evaluate our model's robustness and deepen our understanding of signal behavior, we conducted extensive simulations testing uncontrolled signal conditions across diverse parameter settings. Figure 4 describes the probability density functions of the channel gain received at D_j are analyzed in detail for different configurations. The analysis covers multiple antenna arrangements $T = \{1, 3, 6, 9, 20, 50\}$, various scale parameters $\Omega_{SD_j} = \{0.5, 1, 2, 4\}$, and different fading scenarios - specifically Nakagami-m fading with $m_{SD_j} = \{0.5, 1, 2, 4\}$ and Rician fading with $K_{SD_j} = \{0, 3, 9\}$. Similar to those of subsection 3.1, the PDF distributions reveal several noteworthy characteristics. When examining the single-antenna configuration (T = 1), the channel gain distribution between S and D_j adheres to traditional fading patterns. Specifically, the Nakagami-m distribution is defined by its shape parameter m_{SD_j} , while the Rician distribution is characterized by K_{SD_j} .

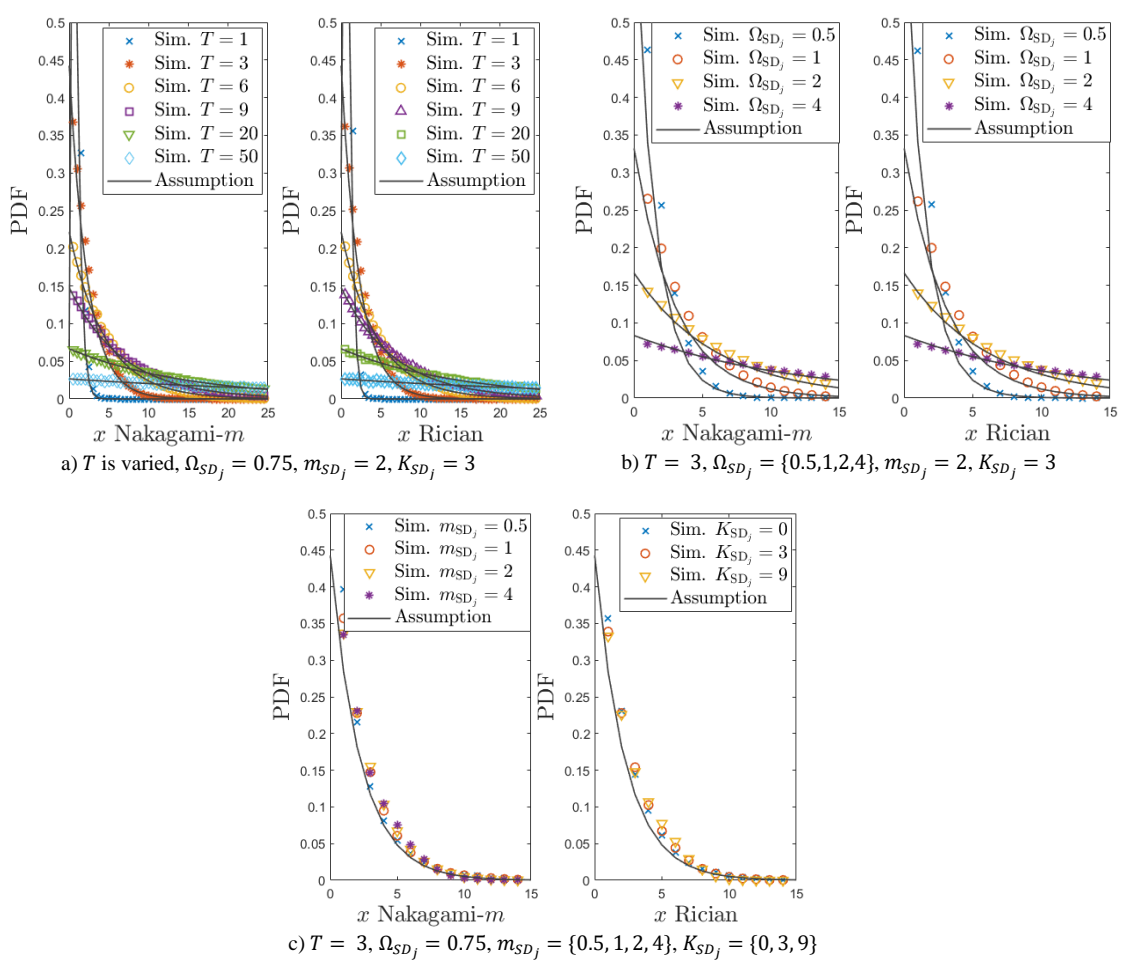


Figure 4. PDF for interference in non-spatial signal processing scenario.

This follows naturally from the inability to implement beamforming in single-antenna systems. For the three-antenna setup (T=3), there are minor deviations between simulated and theoretical results for $\left|\mathbf{h}_{SD_j}\mathbf{w}_{SD_j}^{\dagger}\right|^2$. Specifically, the probability density shows slightly lower values in the lower range of x and marginally higher values in the upper range. However, these differences are minimal when considering the overall distribution pattern. A key observation emerges when comparing the multiple-antenna configurations, i.e. T=3, T=6, and T=9, the results are virtually identical. This similarity strongly suggests that $\left|\mathbf{h}_{SD_j}\mathbf{w}_{SD_j}^{\dagger}\right|^2$ approaches an exponential distribution as the number of antennas increases.

Moreover, Figure 4(b) shows the analysis of the probability density functions of channel gains through both simulation and theoretical approaches, with the following parameters: three transmit antennas (T=3), Nakagami-m shape parameter $m_{SD_j} = 2$, Rician factor $K_{SD_j} = 3$, and varying scale parameters $\Omega_{SD_j} = \{0.5,1,2,4\}$. The results demonstrate that the distributions consistently approximate an exponential pattern with corresponding scale parameters. Notably, our theoretical predictions align closely with the simulation outcomes.

In addition, Figure 4(c) demonstrates the attained channel gain distributions with three antennas (T=3) and scale parameter $\Omega_{SD_j} = 0.75$ across different fading scenarios: Nakagami-m with $m_{SD_j} = \{0.5,1,2,4\}$ and Rician with $K_{SD_j} = \{0,3,9\}$. The results confirm that $\left|\mathbf{h}_{SD_j}\mathbf{w}_{SD_j}^{\dagger}\right|^2$ rapidly converges to an exponential distribution, with only minimal deviations between theoretical predictions and simulations across all values of x.On the other hand, our theoretical framework's feasibility has been also validated through comprehensive simulations that examine the cumulative distribution function characteristics across different system configurations and fading distributions. The simulations explore how the CDF behavior is influenced by three key parameters: the number of antennas (T), the scale parameter Ω_{SD_j} , and the Nakagami-m and Rician fading parameters $(m_{SD_j}$ and $K_{SD_j})$. The effects of these parameters on the CDF are illustrated in Figures 5(a), 5(b), and 5(c), respectively, where the simulation results are in perfect agreement with the analytical expression given in (9).

For the antenna configuration analysis given in Figure 5(a), simulations with $T = \{1, 3, 6, 9, 20, 50\}$ reveal distinct patterns. When T=1, the results still align with traditional Nakagami-m and Rician fading characteristics. However, as T increases to greater than 1, says 3, 6, 9, and so on, the distribution strongly converges toward an exponential distribution, with its scale parameter determined by the product of complex variables and the original scale parameter. Notably, the minimal difference between T=3 and T=9 cases suggests that convergence occurs with relatively few antennas.

Moreover, Figure 5(b) implies that the impact of varying scale parameters Ω_{SD_j} demonstrates consistent agreement with theoretical predictions. Changes in Ω_{SD_j} significantly affect the distribution characteristics, as expected from the theoretical model where the scale parameter directly influences the distribution properties.

Finally, examining the fading parameters (i.e. m_{SD_j} for Nakagami-m and K_{SD_j} for Rician) shown in Figure 5(c) reveals a significant finding: regardless of their values, the interference CDF in non-spatial signal processing systems can be effectively approximated by an exponential distribution with the updated scale parameter. This observation holds true across different fading conditions, providing a valuable simplification for system analysis.

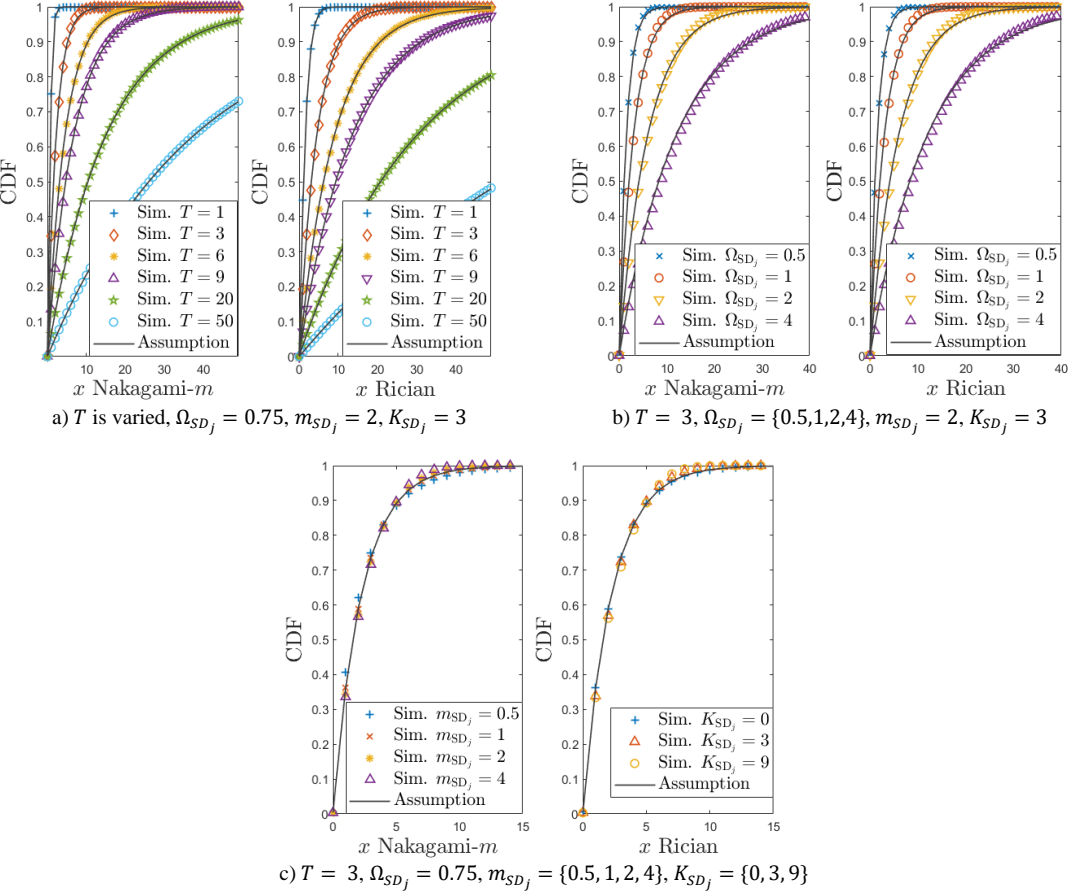


Figure 5. CDF for interference in non-spatial signal processing scenario.

4. CONCLUSIONS

In this paper, we propose an estimation method based on a closed-form expression to analyse the consistent convergence patterns of complex variables in multi-antenna communication systems subjected to fading channels, achieving high accuracy even with few antenna arrays. This work provides comprehensive simulation results to demonstrate the robust convergence of the sum of complex fading channels in multi-antenna communication systems, which include the distribution of interference from both the spatial signal processing scenario and the non-spatial signal processing scenario. Specifically, the distribution of interference from the spatial signal processing schemes over Nakagami-m/Ricican fading channels will strongly converge to an exponential distribution with a constant scale parameter, while that of the non-spatial signal processing systems under similar fading settings also tends to an exponential distribution with a new scale parameter exactly equal to the product of the number of antennas and the scale parameter. Herein, numerical results demonstrate that the PDF of the channel gain and the appropriate CDF are highly converged. As a result, a general approximation based on our results can be used to derive closed-form expressions in more complex situations as well as models in future multi-antenna models, instead of an assumption with a large number of random complex variables to use the central limit theorem.

REFERENCES

- 1. Jiang, W.; Han, B.; Habibi, M.A.; Schotten, H.D. The road towards 6G: A comprehensive survey. IEEE Open Journal of the Communications Society 2021, **2**, 334–366.
- 2. De Alwis, C.; Kalla, A.; Pham, Q.V.; Kumar, P.; Dev, K.; Hwang, W.J.; Liyanage, M. Survey on 6G frontiers: Trends, applications, requirements, technologies and future research. IEEE Open Journal of the Communications Society 2021, **2**, 836–886.
- 3. Alsabah, M.; Naser, M.A.; Mahmmod, B.M.; Abdulhussain, S.H.; Eissa, M.R.; Al-Baidhani, A.; Noordin, N.K.; Sait, S.M.; Al-Utaibi, K.A.; Hashim, F. 6G Wireless Communications Networks: A Comprehensive Survey. IEEE Access 2021, **9**, 148191–148243. https://doi.org/10.1109/324/ACCESS.2021.3124812.
- 4. Sefati, S.S.; Halunga, S. Ultra-reliability and low-latency communications on the Internet of things based on 5G network: Literature review, classification, and future research view. Transactions on Emerging Telecommunications Technologies 2023, **34**, e4770.
- 5. Islam, S.; Atallah, Z.A.; Budati, A.K.; Hasan, M.K.; Kolandaisamy, R.; Nurhizam, S. Mobile Networks Toward 5G/6G: Network Architecture, Opportunities and Challenges in Smart City. IEEE Open Journal of the Communications Society 2024.
- 6. Pons, M.; Valenzuela, E.; Rodríguez, B.; Nolazco-Flores, J.A.; Del-Valle-Soto, C. Utilization of 5G technologies in IoT applications: Current limitations by interference and network optimization difficulties—A review. Sensors 2023, **23**, 3876.
- 7. Antoniewicz, B.; Dreyfus, S. Techniques on Controlling Bandwidth and Energy Consumption for 5G and 6G Wireless Communication Systems. International Journal of communication and computer Technologies 2024, 12, 11–20.
- 8. Rehman, S.U.; Ahmad, J.; Manzar, A.; Moinuddin, M. Beamforming techniques for MIMO-NOMA for 5G and beyond 5G: Research gaps and future directions. Circuits, Systems, and Signal Processing 2024, **43**, 1518–1548.
- 9. B. Praveen Kumar and U. K. Kommuri, "Review on 5G Small Cell Base Station Antennas: Design Challenges and Technologies," in IEEE Access, **12**, pp. 85899-85928, 2024, doi: 10.1109/ACCESS.2024.3415640.
- 10. Kwak, S.; Kim, J. Central limit theorem: The cornerstone of modern statistics. Korean Journal of Anesthesiology 2017, **70**, 144. https://doi.org/10.4097/kjae.2017.70.2.144.
- 11. Zhang, X.; Astivia, O.L.O.; Kroc, E.; Zumbo, B.D. How to Think Clearly About the Central Limit Theorem. Psychological Methods 2023, **28**, 1427–1445. https://doi.org/10.1037/met0000448.
- 12. Hanif, M.F.; Ding, Z.; Ratnarajah, T.; Karagiannidis, G.K. A Minorization-Maximization Method for Optimizing Sum Rate in the Downlink of Non-Orthogonal Multiple Access Systems. IEEE Transactions on Signal Processing 2016, **64**, 76–88. https://doi.org/10.1109/TSP.2015.2480042.
- 13. Moustakas, A.; Simon, S.; Sengupta, A. MIMO capacity through correlated channels in the presence of correlated interferers and noise: a (not so) large N analysis. IEEE Transactions on Information Theory 2003, **49**, 2545–2561. https://doi.org/10.1109/TIT.2003.817427.

- 14. Jung, M.; Kim, T.; Min, K.; Kim, Y.; Lee, J.; Choi, S. Asymptotic Distribution of System Capacity in Multiuser MIMO Systems with Large Number of Antennas. In Proceedings of the 2013 IEEE 77th Vehicular Technology Conference (VTC Spring), 2013, pp. 1–5. https://doi.org/10.1109/VTCSpring.2013.6692462.
- 15. López, O.L.A.; Alves, H.; Souza, R.D.; Montejo-Sánchez, S. Statistical Analysis of Multiple Antenna Strategies for Wireless Energy Transfer. IEEE Transactions on Communications 2019, 67, 7245–7262. https://doi.org/10.1109/TCOMM.2019.2928542.
- 16. Kammoun, A.; Kharouf, M.; Hachem, W.; Najim, J. A Central Limit Theorem for the SINR at the LMMSE Estimator Output for Large Dimensional Signals. IEEE Transactions on Information Theory 2008, **55**. https://doi.org/10.1109/TIT.2009.2030463.
- 17. Hu, J.; Li, W.; Zhou, W. Central Limit Theorem for Mutual Information of Large MIMO Systems With Elliptically Correlated Channels. IEEE Transactions on Information Theory 2019, **65**, 7168–7180. https://doi.org/10.1109/TIT.2019.2913760.
- 18. Ullah, M.S.; Ashraf, Z.B.; Sarker, S.C. Performance Analysis of 6G Multiuser Massive MIMO-OFDM THz Wireless Systems with Hybrid Beamforming under Intercarrier Interference. arXiv preprint arXiv:2401.12351 2024.
- 19. Gao, M.; Li, Y.; Dobre, O.; Al-Dhahir, N. Blind Identification of SFBC-OFDM Signals Based on the Central Limit Theorem. IEEE Transactions on Wireless Communications 2019, PP, 1–1. https://doi.org/10.1109/TWC.2019.2914687.
- 20. Hajiabadi, M.E.; Mashhadi, H.R. Analysis of the Probability Distribution of LMP by Central Limit Theorem. IEEE Transactions on Power Systems 2013, **28**, 2862–2871. https://doi.org/10.1109/TPWRS.2013.2252372.